Co-doping of Al and Bi to control the transport properties for improving thermoelectric performance of Mg₂Si

CrossMark

Gwansik Kim [a], Jeongmin Kim [a], Hwijong Lee [a], Sungmee Cho [a], Inwoong Lyo [b], Sujung Noh [b], Byung-Wook Kim [b], Sung Wng Kim [c], Kyu Hyoung Lee [d,*], Wooyoung Lee [a,*]

[a] Department of Materials Science and Engineering, Yonsei University, Seoul 120-749, South Korea
[b] Advanced Materials Research Team, Central Advanced Research and Engineering Institute, Hyundai Motor Company, Uiwang 437-718, South Korea
[c] Department of Energy Science, Sungkyunkwan University, Suwon 440-746, South Korea
[d] Department of Nano Applied Engineering, Kangwon National University, Chuncheon 200-701, South Korea

ARTICLE INFO

ABSTRACT

We investigated the thermoelectric properties of Al and Bi co-doped Mg₂Si polycrystalline bulks fabricated using a solid state reaction combined with the spark plasma sintering technique. Through controlled doping of Al and Bi, the power factor could be enhanced due to an increase in the Seebeck coefficient benefiting from an enhancement of the density of states effective mass. The lattice thermal conductivity was reduced due to intensified point-defect phonon scattering originating from the mass difference between the host Si atoms and Bi dopants. By these synergetic effects, the dimensionless figure of merit (ZT) of 1.02 was obtained at 873 K.

© 2016 Elsevier Ltd. All rights reserved.

1. Introduction

Thermoelectric power generation (TEG) from waste heat has received renewed attention as a renewable energy source. Among TEG applications, recent efforts are focused on the development of an automotive TE generator (ATEG), due to the increased societal needs for improving the fuel efficiency of a vehicle. However, high-performance bulk-type materials with good operational reliability are essential for the commercialization of ATEG because the performance of TEG system is highly dependent on the conversion efficiency of TE materials. The conversion efficiency is evaluated using the dimensionless figure of merit $ZT = \sigma S^2 T/\kappa_{tot}$, where σ is the electrical conductivity, S is the Seebeck coefficient, and κ_{tot} is the total thermal conductivity at a given absolute temperature T.

Recently, ZT values of various candidate materials for ATEG, including Bi₂Te₃-, [1] PbTe-, [2,3] Skutterudite-, [4] half-Heusler-, [5,6] and Mg₂Si-based materials, [7] have been largely enhanced by the introduction of nanotechnology. Fabrication of nanostructured materials, such as nanograined composites and nanoinclusion composites, offers the possibility of controlling both electronic and thermal transport properties in the presence of highly dense grain and/or phase boundaries [8]. Another approach to enhance ZT is the formation of point defects by substitutional doping. This has been the most general way to improve the power factor (σS^2) by optimization of carrier concentration (n_c) and/or to reduce the lattice thermal conductivity ($\kappa_{lat} = \kappa_{tot} - \kappa_{ele}$, where κ_{ele} is the electronic contribution of thermal conduction), due to the intensified point defect phonon scattering that originates from the mass difference between host atoms and dopants [9,10]. However, this compositional tuning approach is much more complicated, since the electronic and thermal transport properties are interrelated. Thus, the establishment of doping strategies based on the analysis of lattice dynamics and electronic structures is a vital issue in TE materials.

Mg₂Si-based TE materials provide very attractive device-fabricating factors as promising candidates for ATEG: (1) abundance and non-toxicity of their constituent elements and (2) low weight load due to having the lowest density (~1.99 g/cm³) among TE materials. Undoped Mg₂Si is a narrow-bandgap (~0.77 eV) semiconductor, [11] and its ZT value is very low (~0.1) [12]. However, it becomes an effective n-type TE material with a significantly enhanced value of $ZT > 1.0$ when alloyed with a small amount of dopants such as Sn [13,14]. Recent experimental and theoretical results suggest that the high TE performance of Mg₂Si₁₋ₓSnₓ originates from the convergence of electronic bands and the reduction of κ_{lat} [15–17]. Thus, the effect of various doping elements on TE transport properties of Mg₂Si has been extensively studied for more enhanced ZT. Al and Bi are also known to be effective doping elements for enhancing TE performance of Mg₂Si; both doped Al at Mg sites and Bi at Si sites enhance the power factor by generating electron carriers, [18] and Bi-doping also reduces κ_{lat} by mass fluctuation [19].

However, the TE properties of Al and Bi co-doped Mg_2Si are rarely investigated, due to the difficulty of reaction control and the solubility limit of Bi.

In the present study, we fabricated Al and Bi co-doped Mg_2Si polycrystalline bulks and investigated their electronic and thermal transport properties, expecting that such multiple doping would enhance the TE performance. A systematic doping strategy for manipulation of each transport phenomenon was derived from the calculation of transport parameters and the analysis of phase formation. We found that the solubility limit of Bi on Si sites could be increased by Al addition on Mg sites, which implies that phase formation behavior would be controlled. It was demonstrated that a high power factor of 2.9 mW m^{-1} K^{-2} and low κ_{lat} of 0.88 W m^{-1} K^{-1} at 873 K could be achieved by co-doping of Al and Bi, and the largest ZT of 1.02 at 873 K was obtained in $Mg_{1.96}Al_{0.04}Si_{0.97}Bi_{0.03}$ due to the synergetic effects of an increase in power factor by engineering of density of states (DOS) and a decrease in κ_{lat} by intensified point-defect phonon scattering.

2. Experiment

Al- and Bi-doped Mg_2Si polycrystalline bulks with compositions of $Mg_{2-x}Al_xSi_{1-y}Bi_y$ ($x = 0, 0.02, 0.04$; $y = 0, 0.03, 0.04$) were fabricated by a conventional solid state reaction combined with a spark plasma sintering (SPS) technique. Commercial high-purity Mg (99.98%, Aldrich), Si (99.9%, Alfa Aesar), Al (99.5%, Alfa Aesar), and Bi (99.999%, Alfa Aesar) were weighed in the proper ratio of the required composition, and Mg was added with an excess of 5 wt.% of stoichiometric amount for a supplementation of Mg ions on the vacant Mg sites generated by the volatilization during the solid state reaction process. The starting materials were mixed for 1 h in a glove box using an agate mortar. The mixtures were cold-pressed under 40 MPa into disks before a 2-step solid state reaction. For the formation of solid solution compounds, the first heat treatment was conducted in a tube-type furnace under dynamic vacuum at 673 K for 1 h, then heated to 823 K for 1 h, and finally maintained at 823 K for 6 h in order to improve the homogeneity. Acquired samples were crushed into powder using a ball mill (8000D, SPEX, USA) for 5 min. Milled powders were separated by sieving to obtain <53 μm diameter particles. To form highly dense polycrystalline bulks, disk-shaped samples (10 mm in diameter and 2 mm in thickness) were prepared by SPS under 40 MPa at 1023 K for 5 min in vacuum. The densities (ρ_s) of SPSed samples ranged from 1.94 g cm^{-3} to 2.04 g cm^{-3} (> 96% of theoretical density).

Phase analysis of the SPSed bulks was carried out using the X-ray diffraction method (Ultima IV/ME 200DX, Rigaku, Japan) with CuKα radiation. Structural factors obtained from the X-ray diffraction data were refined by the Rietveld method by using the FULLPROF suite. Hall effect measurements were carried out in the van der Pauw configuration under a constant magnetic field (1 T). The Hall mobility (μ_{Hall}) and n_c were calculated using a one-band model. The σ and S values from 373 K to 873 K were measured using a TE property measurement system (ZEM-3, ULVAC, Japan). The κ_{tot} values ($\kappa_{tot} = \rho_s C_p \lambda$) were calculated from measurements taken separately: λ values were measured under vacuum using the laser flash method (Netzsch LFA-457, Germany), in which the heat capacity (C_p) was used as the constant value of 840 J g^{-1} K^{-1} measured using differential scanning calorimetry (DSC 8000, Perkin Elmer, USA).

3. Results and discussion

Fig. 1 shows the X-ray diffraction patterns for Bi-doped and Al and Bi co-doped Mg_2Si compounds. All patterns are indexed with a targeted cubic Fm3m space group as a major phase, and the minor secondary phase MgO is detected in all compositions due to the oxidation of Mg during the solid state reaction. On the other hand, Bi_2Mg_3 and Si are observed in the Bi-doped sample ($Mg_2Si_{0.97}Bi_{0.03}$), suggesting the limited solubility of Bi. Although single-phase Bi-doped Mg_2Si could be formed
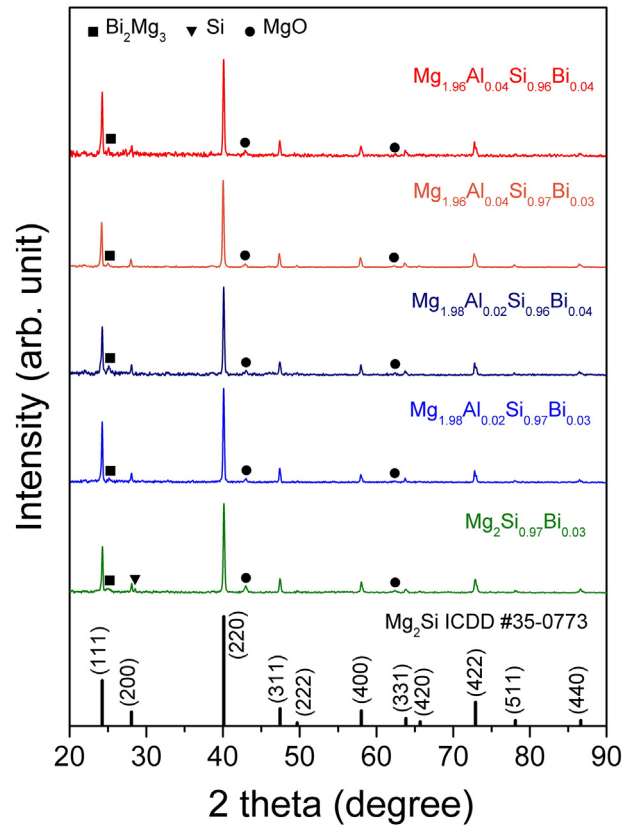
Fig. 1. The XRD patterns for $Mg_{2-x}Al_xSi_{1-y}Bi_y$ ($x = 0, 0.02, 0.04, y = 0.03, 0.04$) spark plasma sintered bulks.

by additional processes, such as long-time post annealing, [20] simpler and more scalable approaches to enlargement of Bi-doping content are highly necessary for cost-effective mass production. Based on a conventional solid state reaction process, we tried to increase Bi solubility through compositional tuning without any complementary synthetic procedure. We selected Al as a co-doping element for simultaneous control of the phase formation and electronic structure of Bi-doped Mg_2Si. We found that the formation of Bi_2Mg_3 could be controlled by Al-doping. As shown in Fig. 1, the wt.% of Bi_2Mg_3, which was calculated using Rietveld refinement, was largely reduced in $Mg_{1.98}Al_{0.02}Si_{0.96}Bi_{0.03}$ (~2.1 wt.%) and $Mg_{1.96}Al_{0.04}Si_{0.96}Bi_{0.03}$ (~1.8 wt.%) compared to that of $Mg_2Si_{0.97}Bi_{0.03}$ (~3.7 wt.%), suggesting increased Bi-doping content by Al addition.

A scanning electron microscopy (SEM) image for the fractured surface of $Mg_{1.96}Al_{0.04}Si_{0.96}Bi_{0.03}$ (Fig. 2(a)) revealed the polycrystalline nature of the bulk, with an average grain size of ~10 μm. Bi_2Mg_3 precipitates (0.1–1 μm) were also observed in the matrix. STEM (scanning transmission electron microscopy)-HAADF (high-angle annular darkfield) analysis was also performed in order to clarify the location of Bi atoms. The preferred occupancy of doped Al at Mg sites has been demonstrated in many previous studies. [21,22] Fig. 2(b) shows the STEM-HAADF images of $Mg_{1.96}Al_{0.04}Si_{0.96}Bi_{0.03}$ along the [110] zone axis. Randomly distributed atomic columns with brighter intensity (blue circles) are clearly observed at Si sites, indicating that doped Bi atoms are located on the Si atoms. Thus, the electron carriers might be generated by both Bi^{5+}-doping at Si^{4+} sites and Al^{3+}-doping at Mg^{2+} sites.

Fig. 3(a) shows the temperature dependence of σ for $Mg_{2-x}Al_xSi_{1-y}Bi_y$ ($x = 0, 0.02, 0.04$; $y = 0.03, 0.04$). We prepared three different samples of each composition, as well as a pristine Mg_2Si sample, to examine the effect of the doping and its reproducibility. The σ values of the three $Mg_2Si_{0.97}Bi_{0.03}$ samples show high irreproducibility, as shown in Fig. 3(a), while the reproducibility of the σ values is significantly
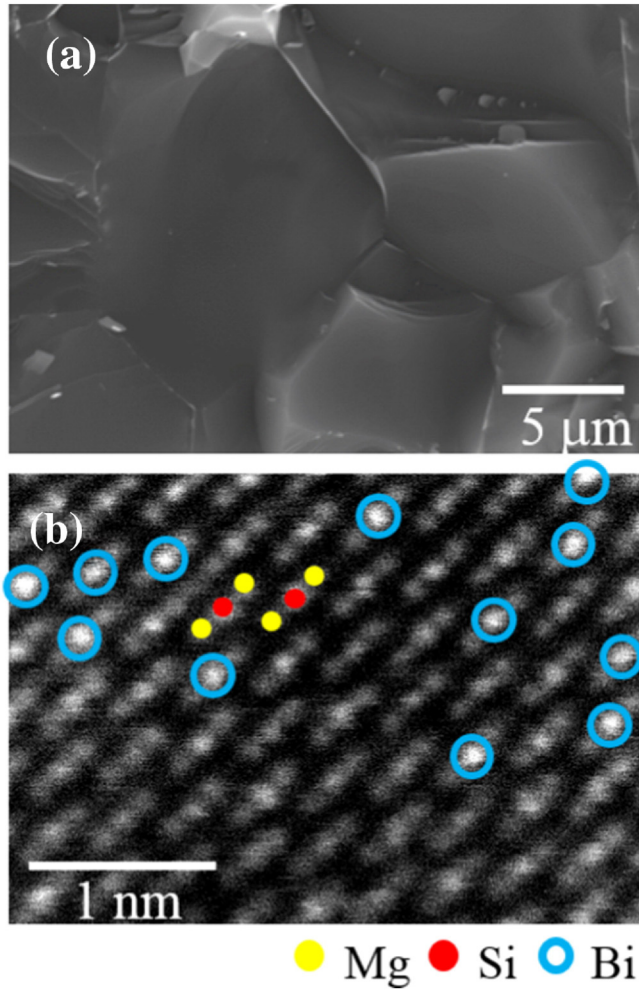
Fig. 2. (a) SEM image of the fractured surface of $Mg_{1.96}Al_{0.04}Si_{0.97}Bi_{0.03}$ (b) STEM-HAADF image of $Mg_{1.96}Al_{0.04}Si_{0.97}Bi_{0.03}$. (For interpretation of the references to color in this figure legend, the reader is referred to the web version of this article.)

Fig. 3. Temperature dependence of (a) electrical conductivity and (b) Seebeck coefficient for $Mg_{2-x}Al_xSi_{1-y}Bi_y$ ($x = 0, 0.02, 0.04; y = 0.03, 0.04$). The inset in (b) shows the temperature dependence of the power factor. (c) Seebeck coefficient as a function of carrier concentration (Pisarenko plot) at 873 K for $Mg_{2-x}Al_xSi_{1-y}Bi_y$ ($x = 0, 0.02, 0.04; y = 0.03, 0.04$).

improved by Al-doping; the σ values of the three samples of all Al and Bi co-doped compositions exhibit much smaller error bars. This result suggests that the reaction of Bi-doping could be stabilized by Al addition, even in our simple solid state reaction. On the other hand, the σ value of undoped Mg_2Si was very low (~935 S m^{-1} at 373 K), while the values of σ were largely increased by both Al- and Bi-doping. These results indicate that Al^{3+} at Mg^{2+} sites and Bi^{5+} at Si^{4+} sites act as electron donors. In order to clarify the behavior of σ, we evaluated n_c and μ_{Hall} at 300 K and listed their values in Table 1. $Mg_{1.96}Al_{0.04}Si_{0.96}Bi_{0.03}$ exhibits higher σ values at lower temperature than do $Mg_2Si_{0.97}Bi_{0.03}$ and the 1 at.% Al-doped compositions ($Mg_{1.98}Al_{0.02}Si_{0.97}Bi_{0.03}$ and $Mg_{1.98}Al_{0.02}Si_{0.96}Bi_{0.04}$), due to its larger n_c (~1.14×10^{20} cm^{-3}) and higher μ_{Hall} (~70.2 cm^2 V^{-1} s^{-1}) value. Meanwhile, $Mg_{1.96}Al_{0.04}Si_{0.96}Bi_{0.04}$ shows rather lower σ values despite its similar n_c (~1.11×10^{20} cm^{-3}), due to μ_{Hall} (~62.3 cm^2 V^{-1} s^{-1}) being reduced by intensified impurity (p-type semiconducting Bi_2Mg_3) [23] electron scattering. At $T \geq 673$ K, all Al and Bi co-doped compounds show nearly the same values.

Fig. 3(b) shows the temperature dependence of S for $Mg_{2-x}Al_xSi_{1-y}Bi_y$ ($x = 0, 0.02, 0.04; y = 0.03, 0.04$). All samples showed negative S, indicating that the samples were n-type semiconductors. The temperature dependence of S for the Al and Bi co-doped compounds was similar to that for the reference $Mg_2Si_{0.97}Bi_{0.03}$, whereas the absolute value of S decreased with increased Al-doping, mainly due to the increase in n_c. However, the decrease of the S was rather small considering the level of the increase in n_c. This is clearly seen in the plot of power

Table. 1
Room temperature values of the carrier concentration (n_c) and mobility (μ_{Hall}) for $Mg_{2-x}Al_xSi_{1-y}Bi_y$ ($x = 0, 0.02, 0.04; y = 0.03, 0.04$).

	n_c (cm^{-3})	μ_{Hall} (cm^2 Vs^{-1})
$Mg_{1.96}Al_{0.04}Si_{0.96}Bi_{0.04}$	1.11×10^{20}	62.3
$Mg_{1.96}Al_{0.04}Si_{0.97}Bi_{0.03}$	1.14×10^{20}	70.2
$Mg_{1.98}Al_{0.02}Si_{0.96}Bi_{0.04}$	9.68×10^{19}	65.3
$Mg_{1.98}Al_{0.02}Si_{0.97}Bi_{0.03}$	8.91×10^{19}	76.6
$Mg_2Si_{0.97}Bi_{0.03}$	5.12×10^{19}	59.5

factor values, as shown in the inset of Fig. 3(b). Compared with the reference $Mg_2Si_{0.97}Bi_{0.03}$ (~2.44 mW m^{-1} K^{-2} at 873 K), enhanced power factor values of ~2.9 mW m^{-1} K^{-2} at 873 K were obtained in Al and Bi co-doped compounds, suggesting the increase of the DOS near the Fermi level. To clarify the difference in electronic transport behavior between single Bi-doped and Al and Bi co-doped Mg_2Si, we calculated the DOS effective mass value m_d^*. The m_d^* was estimated from the measured S and n_c with the use of the following Eq. (2):

$$S = \frac{8\pi^2 k_B^2}{3eh^2}\left(\frac{\pi}{3n_c}\right)^{2/3} m^* T, \tag{1}$$

where k_B, e, and h are the Boltzmann constant, elementary charge, and the Planck constant, respectively. Fig. 3(c) shows the measured S as a function of n_c for all samples at 873 K. The solid lines are calculated for $m_d^* = 0.3$, 0.5, 0.7, and $0.9m_0$, assuming a single parabolic band and energy-independent carrier scattering approximation for degenerated semiconductors. As shown in Fig. 3(c), m_d^* significantly increases from $0.50m_0$ ($Mg_2Si_{0.97}Bi_{0.03}$) to 0.68–$0.77m_0$ by Al and Bi co-doping. It is believed that the larger m_d^* for Al and Bi co-doped Mg_2Si are due to the enlarged DOS near the Fermi level by band structure modification in association with chemical potential tuning (e.g. resonant state). The increased S is attributed to the larger m_d^*.

Fig. 4(a) shows the temperature dependence of κ_{tot} for $Mg_{2-x}Al_x Si_{1-y}Bi_y$ ($x = 0$, 0.02, 0.04, $y = 0.03$, 0.04). The κ_{tot} values at 373 K of Al and Bi co-doped Mg_2Si were lower (4.03–4.45 W m^{-1} K^{-1}) than that of $Mg_2Si_{0.97}Bi_{0.03}$ (4.81 W m^{-1} K^{-1} at 373 K). As shown in Fig. 4(a), lower κ_{tot} values of Al and Bi co-doped Mg_2Si were maintained even at higher temperatures. Because κ_{tot} contains κ_{ele}, which is ruled by the Wiedemann–Franz law ($\kappa_{ele} = L\sigma T$, where L is the Lorenz number), this is an unexpected result, considering the higher σ of Al and Bi co-doped Mg_2Si. We calculated the κ_{lat} values to elucidate the point defect phonon scattering effect by substituted atoms. The value of κ_{lat} was calculated by subtraction of κ_{ele} from κ_{tot}, where κ_{ele} was estimated using the Wiedemann–Franz law. The Lorenz number L was estimated using the following equation:

$$L_0 = \left(\frac{k_B}{e}\right)^2\left(\frac{(r+7/2)F_{r+5/2}(\eta)}{(r+3/2)F_{r+1/2}(\eta)} - \left[\frac{(r+5/2)F_{r+3/2}(\eta)}{(r+3/2)F_{r+1/2}(\eta)}\right]^2\right), \tag{2}$$

where r is the scattering parameter, which was calculated form the temperature dependence of μ_{Hall}, $F_n(\eta)$ is the n-th order Fermi integral, and η is Fermi energy, respectively. Details of the L calculation have been described elsewhere [24]. The values of L, ranging from 1.98×10^{-8} V^2 K^{-2} to 2.35×10^{-8} V^2 K^{-2}, were found for Bi-doped and Al and Bi co-doped Mg_2Si samples. As shown in Fig. 4(b), κ_{lat} values at 873 K of Al and Bi co-doped Mg_2Si were lower (0.88–1.28 W m^{-1} K^{-1}) than that of $Mg_2Si_{0.97}Bi_{0.03}$ (1.83 W m^{-1} K^{-1}). One possible reason is Al-doping. However, Al at Mg sites would not act as effective phonon scattering centers, due to the similarity in mass ($M_{Al} = 26.98$) to Mg ($M_{Mg} = 24.30$) [25]. Thus, the reduction of κ_{lat} in Al and Bi co-doped Mg_2Si should originate from intensified point defect phonon scattering due to the large mass difference between Si ($M_{Si} = 28.08$) and Bi ($M_{Bi} = 208.98$).

The dimensionless figures of merit ZTs of $Mg_{2-x}Al_xSi_{1-y}Bi_y$ ($x = 0$, 0.02, 0.04; $y = 0.03$, 0.04) are shown in Fig. 4(c). The ZT values were significantly enhanced over a wide temperature range by co-doping of Al and Bi, and the peak ZT value obtained is 1.02 at 873 K for the $Mg_{1.96}Al_{0.04}Si_{0.97}Bi_{0.03}$ sample. These high ZT values are due to the simultaneous manipulation of electronic and thermal transport properties by multiple doping. It is noted that a further enhancement of ZT is possible through the formation of nanostructures, especially those with a larger characteristic length than that of the impurity atoms, allowing reduced κ_{lat} by intensified mid- and long-wavelength phonon scattering.
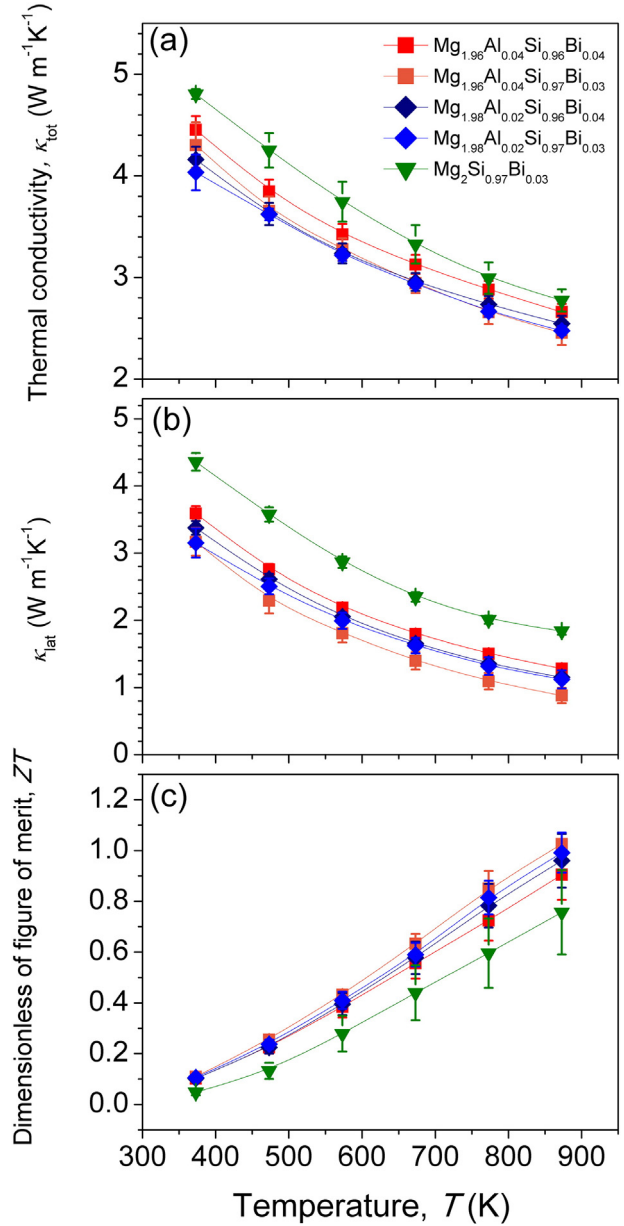
Fig. 4. Temperature dependence of (a) thermal conductivity, (b) lattice thermal conductivity and (c) dimensionless figure merit ZT for $Mg_{2-x}Al_xSi_{1-y}Bi_y$ ($x = 0$, 0.02, 0.04; $y = 0.03$, 0.04).

4. Conclusions

We investigated the phase formation and thermoelectric properties of Al and Bi co-doped Mg_2Si. Al addition at Mg sites stabilized the doping of Bi on Si sites and increased the controllability of electronic and lattice structures. It was found that both electronic and thermal transport properties of Mg_2Si-based thermoelectric materials could be controlled by a compositional tuning approach. Enhanced power factor and reduced lattice thermal conductivity were obtained by co-doping of Al and Bi due to the increased density of states effective mass and intensified point defect phonon scattering. A peak ZT value of 1.02 was observed at 873 K for $Mg_{1.96}Al_{0.04}Si_{0.97}Bi_{0.03}$.

References

[1] M. Zebarjadi, K. Esfarjani, M.S. Dresselhaus, Z.F. Ren, G. Chen, Energy Environ. Sci. 5 (2012) 5147–5162.
[2] G.J. Snyder, E.S. Toberer, Nat. Mater. 7 (2008) 105–114.
[3] Y.Z. Pei, H. Wang, G.J. Snyder, Adv. Mater. 24 (2012) 6125–6135.
[4] J.R. Sootsman, D.Y. Chung, M.G. Kanatzidis, Angew. Chem. Int. Ed. 48 (2009) 8616–8639.
[5] Q. Shen, L. Chen, T. Goto, T. Hirai, J. Yang, G.P. Meisner, C. Uher, Appl. Phys. Lett. 79 (2001) 4165–4167.
[6] W. Liu, X. Yan, G. Chen, Z.F. Ren, Nano Energy 1 (2012) 42–56.
[7] R. Chen, JOM 65 (2013) 702–708.
[8] B. Poudel, Q. Hao, Y. Ma, Y. Lan, A. Minnich, B. Yu, X. Yan, D. Wang, A. Muto, D. Vashaee, X. Chen, J. Liu, M.S. Dresselhaus, G. Chen, Z.F. Ren, Science 320 (2008) 634–638.
[9] J. Callaway, H.C. von Baeyer, Phys. Rev. 120 (1960) 1149–1154.
[10] P.G. Klemens, Phys. Rev. 119 (1960) 507–509.
[11] M. Ioannou, G. Polymeris, E. Hatzikraniotis, A.U. Khan, K.M. Paraskevopoulos, T. Kyratsi, J. Electron. Mater. 42 (2013) 1827–1834.
[12] J. Tani, H. Kido, Intermetallics 15 (2007) 1202–1207.
[13] V.K. Zaitsev, M.I. Fedorov, E.A. Gurieva, I.S. Eremin, P.P. Konstantinov, A.Y. Samunin, M.V. Vedernikov, Phys. Rev. B 74 (2012) 045207.
[14] W. Liu, X.F. Tang, H. Li, K. Yin, J. Sharp, X.Y. Zhou, C. Uher, J. Mater. Chem. 22 (2012) 13653–13661.
[15] W. Liu, X.J. Tan, K. Yin, H.J. Liu, X.F. Tang, J. Shi, Q.J. Zhang, C. Uher, Phys. Rev. Lett. 108 (2012) 166601.
[16] X.H. Liu, T.J. Zhu, H. Wang, L.P. Hu, H.H. Xie, G.Y. Jiang, G.J. Snyder, X.B. Zhao, Adv. Energy Mater. 3 (2013) 1238–1244.
[17] H.L. Gao, T.J. Zhu, X.B. Zhao, Y. Deng, J. Solid State Chem. 220 (2014) 157–162.
[18] J. Tani, H. Kido, Physica B 364 (2005) 218–224.
[19] W. Liu, Q. Zhang, K. Yin, H. Chi, X.Y. Zhou, X.F. Tang, C. Uher, J. Solid State Chem. 203 (2013) 333–339.
[20] M. Ioannou, G.S. Polymeris, E. Hatzikraniotis, K.M. Paraskevopoulos, T. Kyratsi, J. Phys. Chem. Solids 75 (2014) 984–991.
[21] S. Battiston, S. Fiameni, M. Saleemi, S. Boldrini, A. Famengo, F. Agresti, M. Stingaciu, M.S. Toprak, M. Fabrizio, S. Barison, J. Electron. Mater. 42 (2013) 1956–1959.
[22] S. Ji, M. Tanaka, S. Zhang, S. Yamanaka, Inorg. Chem. 51 (2012) 10300–10305.
[23] X. Zhang, H.L. Liu, Q.M. Lu, J.X. Zhang, F.P. Zhang, Appl. Phys. Lett. 103 (2013) 063901.
[24] L.D. Zhao, S.H. Lo, J.Q. He, H. Li, K. Biswas, J. Androulakis, C.I. Wu, T.P. Hogan, D.Y. Chung, V.P. Dravid, M.G. Kanatzidis, J. Am. Chem. Soc. 133 (2011) 20476–20487.
[25] S.W. You, K.H. Park, I.H. Kim, S.M. Choi, W.S. Seo, S.U. Kim, J. Electron. Mater. 41 (2012) 1675–1679.